Thermal annealing-induced enhancement of the field-effect mobility of regioregular poly(3-hexylthiophene) films

Shinuk Cho and Kwanghee Lee[a)]
Center for Polymers and Organic Solids, University of California at Santa Barbara, Santa Barbara, California 93106-5090 and Department of Physics, Pusan National University, Busan 609-735, Korea

Jonathan Yuen, Guangming Wang, Daniel Moses, and Alan J. Heeger
Center for Polymers and Organic Solids, University of California at Santa Barbara, Santa Barbara, California 93106-5090

Mathieu Surin and Roberto Lazzaroni
Chemistry of Novel Materials, University of Mons-Hainaut, 20 Place du Parc, 7000 Mons, Belgium

(Received 1 February 2006; accepted 2 October 2006; published online 5 December 2006)

Polymer field-effect transistors with a field-effect mobility of $\mu \approx 0.3\ \mathrm{cm^2\,s^{-1}\,V^{-1}}$ have been demonstrated using regioregular poly(3-hexylthiophene) (rr-P3HT). Devices were fabricated by dip coating the semiconducting polymer followed by annealing at 150 °C for 10 min. The heat annealed devices exhibit an increased field-effect mobility compared with the as-prepared devices. Morphology studies and analysis of the channel resistance demonstrate that the annealing process increases the crystallinity of rr-P3HT and improves the contact between the electrodes and the P3HT films, thereby increasing the field-effect mobility of the films. © *2006 American Institute of Physics*.
[DOI: 10.1063/1.2400796]

I. INTRODUCTION

Because of the reasonably high mobility of regioregular poly(3-hexylthiophene) (rr-P3HT) compared with other semiconducting polymers, field-effect transistors (FETs) fabricated with rr-P3HT as the semiconducting polymer have drawn considerable attention as promising components for "plastic electronics."[1–10] rr-P3HT exhibits regioregular head-to-tail coupling of the hexyl side chains and an ordered crystalline lamellar structure with fibrillar morphology.[3] Since self-organized interchain π-π stacking is achieved between the layers in the crystalline regions, rr-P3HT has demonstrated high performance in FETs with field-effect mobility of $\mu \approx 0.1\ \mathrm{cm^2\,s^{-1}\,V^{-1}}$.[7] It is obvious that increasing crystallinity is very crucial to the performance of polymer FETs. Recently, McCulloch *et al.* reported high mobility of $0.7\ \mathrm{cm^2\,s^{-1}\,V^{-1}}$ using a poly(2,5-bis(3-alkylthiophen-2-yl)thieno[3,2-b]thiophene (PBTTT), which was attributed to the high degree of crystallinity of the polymer.[11] Thus, for the rr-P3HT FET, the need to improve the device performance requires the implementation of fabrication techniques and treatment conditions with the goal of increasing the degree of the crystallinity of rr-P3HT.

In contrast with spin-cast films, dip-coated films exhibit higher crystallinity with the direction of the lamellar stacking parallel to the substrate surface (the backbone planes are perpendicular to the substrate).[6,12] Since this stacking direction is more favorable for high-performance FETs than stacking perpendicular to the substrate surface (as typically observed in spin-cast films), FETs fabricated by dip coating the rr-P3HT exhibit better device performance with field-effect mobilities of $\mu \approx 0.2\ \mathrm{cm^2\,s^{-1}\,V^{-1}}$.[6]

Another approach toward improving the crystallinity of the polymeric films is through thermal annealing.[13,14] Recent studies have demonstrated improved crystallinity in heat-treated rr-P3HT films, as inferred from atomic force microscopy (AFM) measurements and optical spectroscopy, and confirmed by x-ray diffraction.[6,8] Polymer solar cells with power conversion efficiencies approaching 5% have been demonstrated by applying postproduction thermal annealing at 150 °C.[15] In the latter study, the improved performance was attributed to the increased crystallinity of the rr-P3HT component and to the improved contact between the polymer and the metal electrode (Al), both of which are caused by the thermal annealing.

Motivated by the success in polymer solar cells, we have applied postproduction heat treatment to polymer FETs fabricated with rr-P3HT. Devices annealed at 150 °C for 10 min exhibit enhanced field-effect mobilities. In particular, the devices using Pt electrodes exhibit mobilities that approach $0.3\ \mathrm{cm^2\,s^{-1}\,V^{-1}}$.

II. EXPERIMENTS

Polymer FETs were fabricated on heavily doped *n*-type silicon (Si) wafers each covered with a thermally grown silicon oxide (SiO_2) layer with thickness of ~200 nm. The doped Si wafer acts as a gate electrode, and the SiO_2 layer functions as the gate insulator. Source and drain electrodes (~50 nm) using Au or Pt were deposited on the SiO_2 layer by e-beam evaporation after depositing a 3 nm titanium (Ti) layer to improve the metal adhesion. The electrodes were patterned by using standard photolithographic methods. Prior to the deposition of rr-P3HT, the SiO_2 layer was treated with

[a)]Author to whom correspondence should be addressed; electronic mail: kwhlee@pusan.ac.kr

 © 2006 American Institute of Physics

Downloaded 18 Dec 2006 to 130.79.117.100. Redistribution subject to AIP license or copyright, see http://jap.aip.org/jap/copyright.jsp

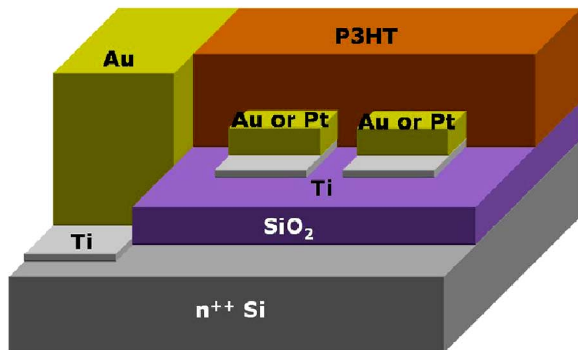

FIG. 1. (Color online) Schematic device structure of bottom-contact FET using rr-P3HT fabricated by dip coating.

the hexamethyldisilazane (HMDS) to convert the surface to be hydrophobic. All FET devices were made in the bottom contact geometry, as shown in Fig. 1.

rr-P3HT (synthesized by the Rieke route) was deposited by dip coating the active layer.[6,12] The molecular weight of our rr-P3HT was determined as 39.5 kD by our own GPC measurement, which is almost comparable with other studies. The concentration of the rr-P3HT in solution in chloroform was 1.0 mg/m*l*, and the dip coating proceeded with the speed of 1 mm/min. The thickness of the P3HT films was about 20 nm. Thermal annealing was carried out on a calibrated and stabilized hot plate under N_2 atmosphere. After annealing, the FETs were placed on a metal plate at room temperature to cool down.

Electrical characterization was performed using a Keithley semiconductor parameteric analyzer (Keithley 4200) under N_2 atmosphere. Film morphology within the channel of the devices were characterized by tapping-mode atomic force microscopy (TM-AFM; Digital Instrument Nanoscope IIIa) operated at room temperature in air.

III. RESULTS AND DISCUSSIONS

Figure 2 shows the transfer characteristics, $|I_{ds}|$ vs V_{gs} and $(|I_{ds}|)^{1/2}$ vs V_{gs} (both at $V_{ds}=-60$ V) for *p*-channel FETs fabricated with Au electrodes [Fig. 2(a)] and with Pt electrodes [Fig. 2(b)], all fabricated by dip coating the rr-P3HT.

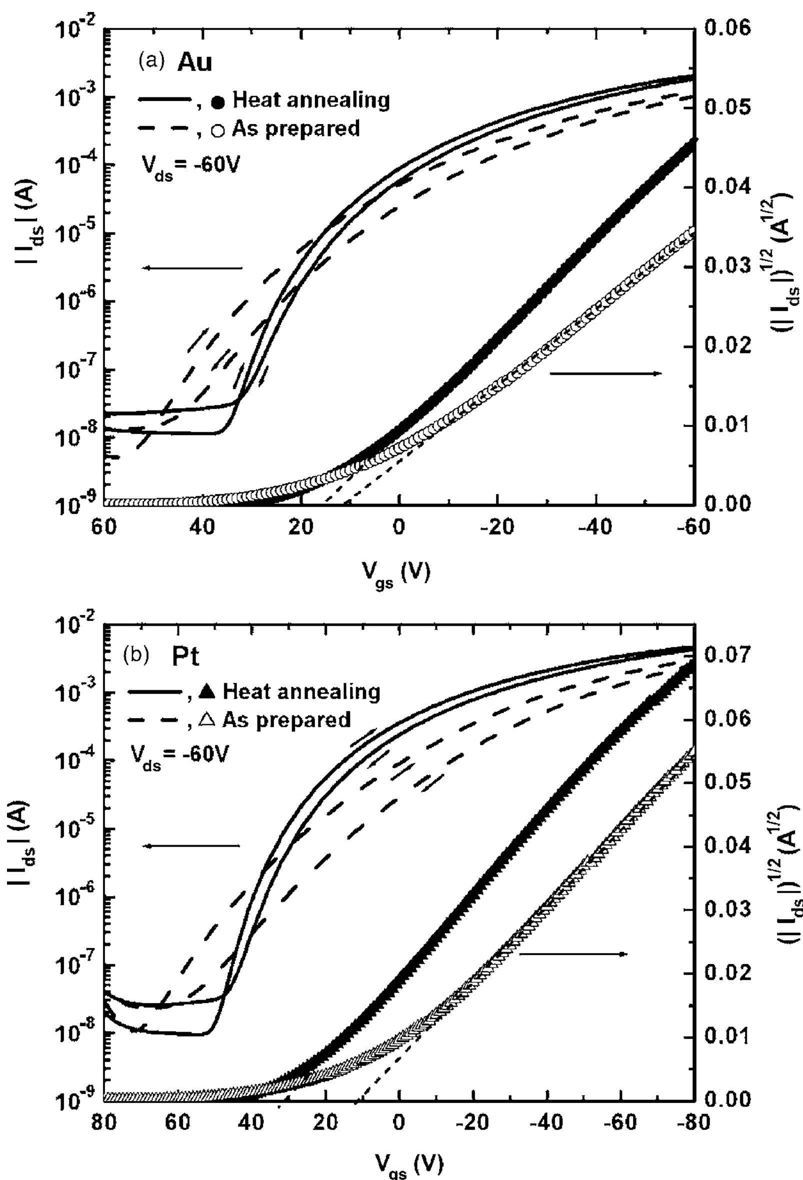

FIG. 2. Comparison of the transfer characteristics ($|I_{ds}|$ vs V_{gs} and $|I_{ds}|^{1/2}$ vs V_{gs}, both measured at $V_{ds}=60$ V) of the rr-P3HT FET devices before and after thermal annealing at 150 °C for 10 min for the devices with (a) Au electrodes and with (b) Pt electrodes.

Downloaded 18 Dec 2006 to 130.79.117.100. Redistribution subject to AIP license or copyright, see http://jap.aip.org/jap/copyright.jsp

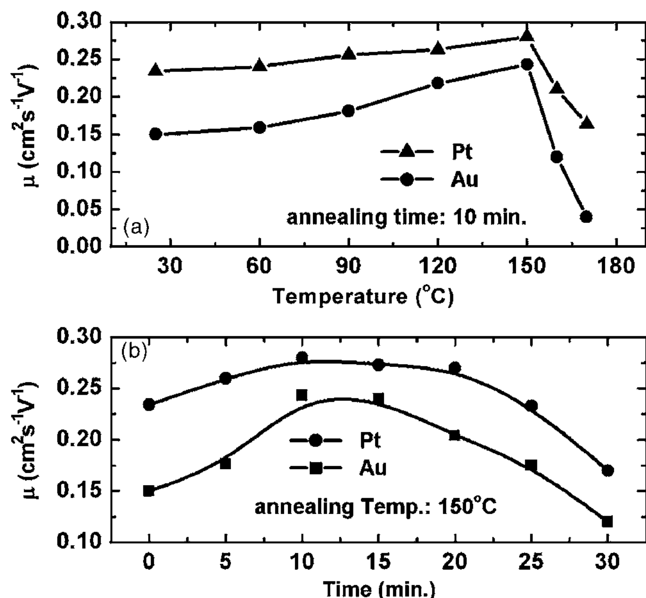

FIG. 3. (a) Field-effect mobility vs annealing temperature with 10 min annealing time, and (b) field-effect mobility vs annealing time at 150 °C for the rr-P3HT FET devices using Au or Pt electrodes. Note that those mobilities are not corrected for the contact resistance.

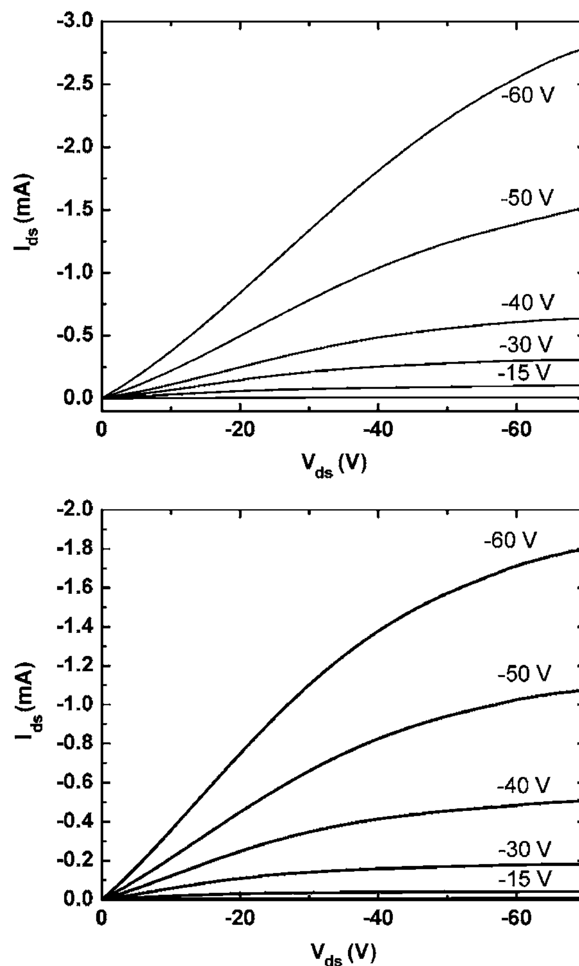

FIG. 4. Example of the output characteristic curves obtained from the most optimized device (annealed at 150 °C for 10 min); (a) Pt electrodes and (b) Au electrodes.

All devices were fabricated using the bottom contact geometry as explained in detail in the Experiments section; all devices were operated in accumulation mode. These I_{ds} vs V_{gs} curves are typical of polymer FETs that have been prepared and subsequently measured at room temperature. Comparison of the data for devices measured with and without prior heat treatment indicates that annealing at 150 °C for 10 min causes an increase in I_{ds}. While the turn-on voltage (V_{to}) moves to lower values for the annealed devices, the threshold voltage (V_T) as obtained from a linear extrapolation of $(|I_{ds}|)^{1/2}$ vs V_{gs}, increases. More importantly, the annealed devices exhibit significantly reduced hysteresis, implying a decrease in the trap density within the transport channel.[16]

The effect of thermal annealing on μ can be inferred from the standard FET relation

$$I_{ds} = (WC_i/2L)\mu(V_{gs} - V_T)^2, \qquad (1)$$

where $W(=1$ mm) is the channel width, and $L(=5\ \mu$m) is the channel length of the devices. Since the devices showed some hysteresis, only up scan data (measured from positive gate bias to negative gate bias) were used to maintain a consistency in the analysis of the data. Figure 3(a) shows a study of μ as a function of the annealing temperature. The mobility increases steadily for annealing temperatures up to 150 °C and then drops abruptly for annealing temperatures above 150 °C. Note the more sensitive dependence on the annealing temperature for the Au-electrode device. The apparently higher μ in the Pt-electrode devices is likely due to the contact resistance at the metal polymer interface; the higher work function of Pt (≈5.6 eV) [compared to Au (≈5.2 eV)] facilitates charge injection. The measured mobility increases by ~60% for the Au-electrode devices and by ~20% for the Pt-electrode devices with the best values approaching 0.3 $cm^2\ s^{-1}\ V^{-1}$. The effect of annealing at 150 °C for different periods of time is also shown in Fig. 3(b). The results reveal that the optimum annealing time is 10–20 min at 150 °C. Figure 4 shows the examples of output characteristic curves obtained from the most optimized devices, which were annealed at 150 °C for 10 min. Figure 4(a) shows the output characteristic curves of the FET fabricated using Pt as the source and drain electrodes, while Fig. 4(b) is to use Au electrodes. Because both output characteristic curves do not show so-called "perfect" saturation as in typical FET devices, it is possible that some overestimation might be made during the process to deduce the mobilities from the curves due to the short channel effects as suggested by Chabinyc *et al.*[16] In fact, the mobilities obtained from larger channel FETs ($L=25\ \mu$m) fabricated with top-contact method show somewhat lower values compared with the short channel FETs; $\mu_e \approx 0.06$ $cm^2\ s^{-1}\ V^{-1}$ for the as-prepared devices and $\mu_e \approx 0.12$ $cm^2\ s^{-1}\ V^{-1}$ for the devices annealed at 150 °C for 10 min. However, the effect of annealing was evident even in such cases.

In order to understand the annealing-induced enhancement in μ, we have directly imaged the corresponding changes in film morphology. Figure 5 shows phase images of the dip-coated rr-P3HT films located within the channel, measured by TM-AFM. The as-prepared film [Fig. 5(a)]

Downloaded 18 Dec 2006 to 130.79.117.100. Redistribution subject to AIP license or copyright, see http://jap.aip.org/jap/copyright.jsp

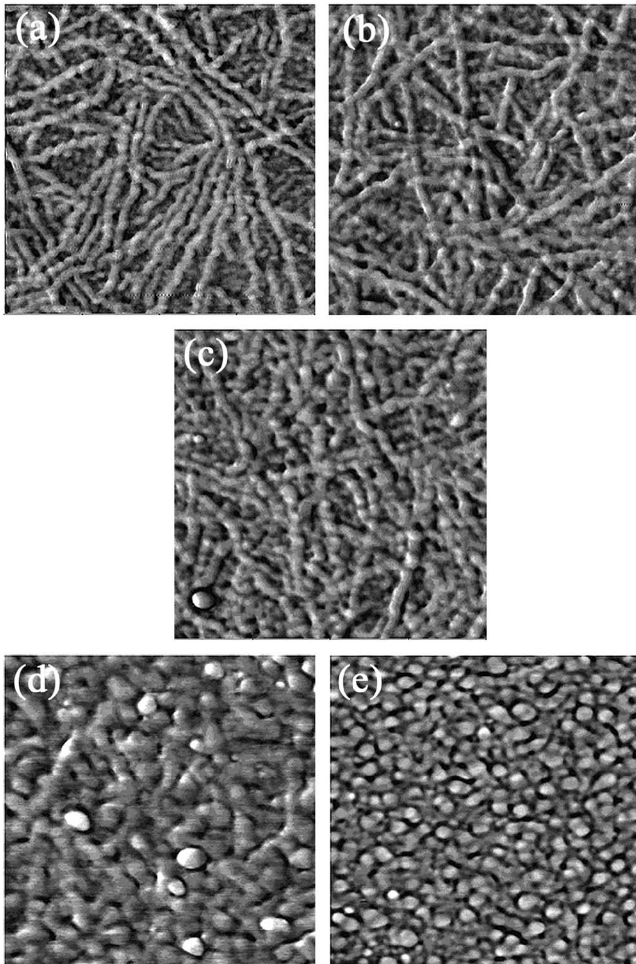

FIG. 5. Tapping-mode AFM phase images (800×800 nm^2) within the FET channel of the dip-coated rr-P3HT FETs; (a) as-prepared and annealed at (b) 150 °C, (c) 160 °C, and (d) 170 °C.

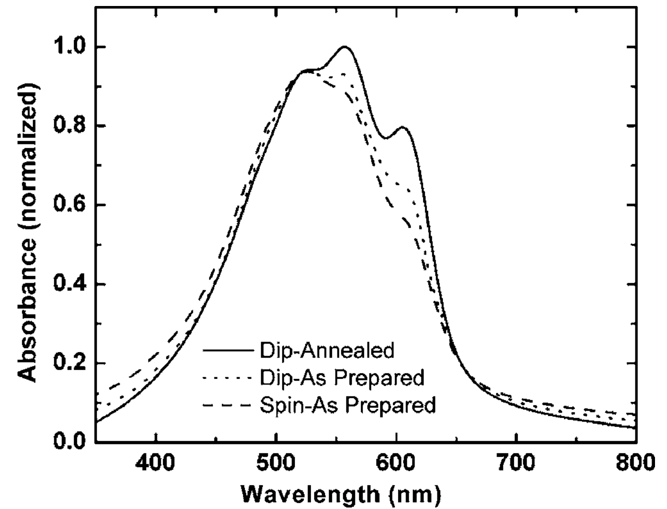

FIG. 6. Absorption spectra of the P3HT thin films fabricated by dip coating. For comparison, the spectrum obtained from the spin coated films is also presented.

shows the characteristic fibrillar morphology of rr-P3HT, in which the crystalline grains with the size of 20–35 nm are embedded along the fibril axis. Early x-ray diffraction studies indicated that the lamellar stacking is parallel to the fibril axis with an interlamellar distance of approximately 1.7 nm within the grains.[17–19] Upon annealing the films at $T \leqslant 150$ °C, these morphological features are preserved, but the thickness of the fibrils increases to 30–40 nm [see Fig. 5(b)], consistent with the annealing temperature dependence of μ; up to 150 °C the crystalline grains become larger and facilitate the charge transport. In addition, the reduced hysteresis of the annealed devices can be attributed to this morphological enhancement because the amount of bulk trap is certainly reduced in such morphologically enhanced films. For $T > 150$ °C, the fibrils first exhibit decomposition into smaller "grains" along the axis [Fig. 5(c) at 160 °C] and then growth of these grains as the annealing temperature increases to 180 °C [Figs. 5(d) and 5(e)]. Thus, the AFM results suggest that a morphological transition from fibrils to grains occurs around 150 °C. Since the grainlike morphology is less favorable than the fibrillar morphology for charge transport, this transition appears to be responsible for the abrupt decrease in μ above 150 °C.[20] We note that sexithienyl films grown under vacuum exhibit a similar morphological transition around 170 °C; the change in morphology was attributed to faster molecular diffusion above this threshold temperature.[21]

Figure 6 shows the absorption spectra obtained from the dip-coated films on fused quartz with and without annealing. For comparison, the spectrum obtained from the spin coated films is presented together. The data show clearly different spectral features for each films prepared with different fabrication conditions. We observed a slight blueshift in the absorption spectrum of the spin-coated film as compared with the dip-coated films. In general, this blueshift is considered as the evidence of formation change inside of polymers.[8,22] On the other hand, comparison of the data for the dip-coated devices measured with and without prior heat treatment indicates that the annealing process causes an increase in the vibronic structures. According to the early study by Hagler *et al.*, the intensity increase of the vibronic structure is originated from the increase of crystallinity.[23] Therefore, we conclude that the heat annealing process induces an increase in the degree of crystallinity of the dip-coated films.

The morphological transition around 150 °C can be directly identified by plotting the route-mean-square (rms) roughness of the rr-P3HT films as a function of the annealing temperature, as shown in Fig. 7. The nonannealed films show a relatively low rms roughness of ~2.5 nm, almost comparable to that of the underlying silicon Si/SiO_2 substrate. Although films annealed at 150 °C show no change in the roughness, films annealed at 155 °C exhibit a sharp increase in the roughness to ~3.8 nm due to the appearance of the grains. The rms roughness decreases again at annealing temperatures around 160 °C and remains unchanged up to 240 °C. We attribute this sudden decrease to the relaxation of the films at temperatures above 160 °C.

As noted above, the contact resistance between rr-P3HT and the electrodes (source and drain) limits the performance in these devices. One might therefore expect that postproduction heat annealing would improve the contact between the rr-P3HT and the electrodes (source and drain). Figure 8(a) shows the total resistance between the source and drain

Downloaded 18 Dec 2006 to 130.79.117.100. Redistribution subject to AIP license or copyright, see http://jap.aip.org/jap/copyright.jsp

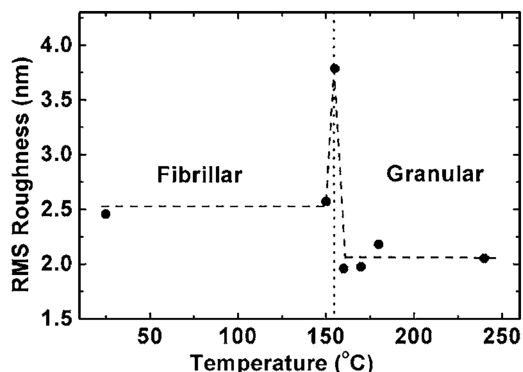

FIG. 7. The evolution of the route-mean-square (rms) roughness of the rr-P3HT films.

(R_{total}) as a function of the channel length (L), as obtained from the linear portion of $I_{ds}-V_{ds}$ curves at various $L(V_{gs}=-60\text{ V})$. In such a case, R_{total} can be expressed as

$$R_{total}=R_s+R_{ch}, \tag{2}$$

where R_s is the sum of the series resistance arising from the contacts between the electrodes (source and drain) and the active layer, and R_{ch} is the channel resistance. Since R_{ch} is proportional to L, we can obtain R_s by the extrapolation of R_{total} vs L to zero channel length as in Fig. 8(a).[24] The results show that the Pt devices (as prepared) have lower R_{total}- values and lower R_s than the Au devices, as expected from the higher work function of Pt. When the devices are annealed at 150 °C for 10 min, R_{total} decreases for both kinds of devices. As noted, thermal annealing increases the degree of crystallinity in the polymers, thereby facilitating the charge transport and lowering R_{ch}. In addition, as shown in the inset of Fig. 8(a), the annealed devices exhibit substantially decreased R_s values compared with the nonannealed devices. In fact, the contact resistances characteristic of polymer FETs are in the range of 10 kΩ–10 MΩ, much larger than those found in inorganic FETs. As a result the contact resistance limits the device performance.[25] Moreover, the R_s values also depend on the gate bias; the magnitude of R_s decreases as the gate bias increases.[24] Although the degree of reduction in R_s for the annealed devices depends on the applied gate bias, as shown in Fig. 8(b), it is obvious that the heat annealing process reduces the magnitude of R_s throughout the applied gate bias between −20 and −80 V. Therefore, our results are encouraging in that the contact resistance problem in polymer FETs can be improved by thermal annealing.

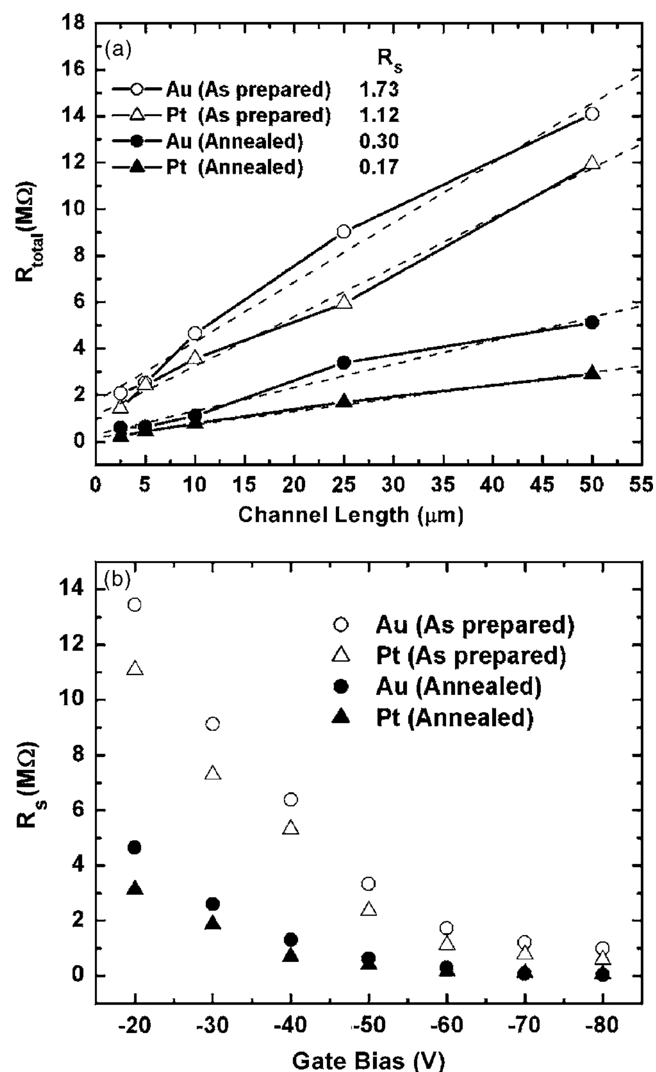

FIG. 8. (a) Total resistance between the source and drain ($R_{total}=R_s+R_{ch}$) as a function of the channel length (L) and (b) series resistance as a function of gate bias.

IV. CONCLUSIONS

In conclusion, we have demonstrated field-effect mobilities approaching 0.3 cm^2 s^{-1} V^{-1} in polymer FETs using rr-P3HT fabricated by dip coating and treated by postproduction thermal annealing. Devices annealed at 150 °C for 10 min exhibit an increased field-effect mobility compared with as-prepared devices. Morphology studies using AFM and analysis of the channel resistance demonstrate that the annealing process increases the crystallinity of rr-P3HT and improves the contact between the electrodes and the P3HT films, thereby increasing the measured field-effect mobility.

ACKNOWLEDGMENTS

The research at UCSB was supported by the Samsung Advanced Institute of Technology. One of the authors (S.C.) acknowledges the financial support from Korea Research Foundation Grant (M07-2004-000-10137-0), and another author (M.S.) acknowledges FRIA (Belgium) for a doctoral fellowship and Communauté française de Belgique for a research stay grant.

[1] F. Padinger, R. Rittberger, and N. S. Sariciftci, Adv. Funct. Mater. **13**, 85 (2003).
[2] X. Yang, J. Loss, S. C. Veenstra, W. J. H. Verhees, M. M. Wienk, J. M. Kroon, M. A. J. Michels, and R. A. J. Janssen, Nano Lett. **5**, 579 (2005).
[3] H. Sirringhaus, N. Tessler, and R. H. Friend, Science **280**, 1741 (1998).
[4] Z. Bao, A. Dodabalapur, and A. J. Lovinger, Appl. Phys. Lett. **69**, 4108 (1996).
[5] C. D. Dimitrakopoulos and P. R. L. Malenfant, Adv. Mater. (Weinheim, Ger.) **14**, 99 (2002).
[6] G. Wang, J. Swensen, D. Moses, and A. J. Heeger, J. Appl. Phys. **93**, 6137 (2003).
[7] H. Sirringhaus *et al.*, Nature (London) **401**, 685 (1999).
[8] A. Zen *et al.*, Adv. Funct. Mater. **14**, 757 (2004).
[9] S. S. Pandey, W. Takashima, S. Nagamatsu, T. Endo, M. Rikukawa, and K. Kaneto, Jpn. J. Appl. Phys., Part 2 **39**, 94 (2003).

Downloaded 18 Dec 2006 to 130.79.117.100. Redistribution subject to AIP license or copyright, see http://jap.aip.org/jap/copyright.jsp

[10] G. Juska, K. Arlauskas, R. Österbacka, and H. Stubb, Synth. Met. **109**, 173 (2000).
[11] I. McCulloch *et al.*, Nat. Mater. **5**, 328 (2006).
[12] G. Wang, T. Hirasa, D. Moses, and A. J. Heeger, Synth. Met. **146**, 127 (2004).
[13] A. J. J. M. van Breemen *et al.*, Adv. Funct. Mater. **15**, 872 (2005).
[14] S. Cho and K. Lee, J. Korean Phys. Soc. **46**, 973 (2005).
[15] W. Ma, C. Y. Yang, X. Gong, K. Lee, and A. J. Heeger, Adv. Funct. Mater. **15**, 1617 (2005).
[16] M. L. Chabinyc, J.-P. Lu, R. A. Street, Y. Wu, P. Liu, and B. S. Ong, J. Appl. Phys. **96**, 2063 (2004).
[17] H. Yang, S. Park, D. Kim, K. Oh, S. Magonov, K. Cho, T. Chang, Z. Bao, and C. Y. Ryu, Polym. Prepr. (Am. Chem. Soc. Div. Polym. Chem.) **44**, 333 (2003).
[18] H. Yang, T. J. Shin, L. Yang, Z. Bao, C. Y. Ryu, and K. Cho, Polym. Prepr. (Am. Chem. Soc. Div. Polym. Chem.) **45**, 212 (2004).
[19] J. A. Merlo and C. D. Frisbie, J. Phys. Chem. B **108**, 19169 (2004).
[20] G. Horowitz and M. E. Hajlaoui, Adv. Mater. (Weinheim, Ger.) **12**, 1046 (2000).
[21] P. Viville, R. Lazzaroni, J. L. Brédas, P. Moretti, P. Samori, and F. Biscarini, Adv. Mater. (Weinheim, Ger.) **10**, 57 (1998).
[22] R. J. Kline, M. D. McGehee, E. N. Kadnikova, J. Liu, J. M. J. Fréchet, and M. F. Toney, Macromolecules **38**, 3312 (2005).
[23] T. W. Hagler, K. Pakbaz, K. F. Voss, and A. J. Heeger, Phys. Rev. B **44**, 8652 (1991).
[24] B. H. Hamadani and D. Natelson, Appl. Phys. Lett. **84**, 443 (2004).
[25] L. Bürgi, T. J. Richards, R. H. Friend, and H. Sirringhaus, J. Appl. Phys. **94**, 6129 (2003).

Downloaded 18 Dec 2006 to 130.79.117.100. Redistribution subject to AIP license or copyright, see http://jap.aip.org/jap/copyright.jsp